The Origin of B-type Runaway Stars: Non-LTE Abundances as a Diagnostic

Published in:
The Astrophysical Journal

Document Version:
Publisher's PDF, also known as Version of record

Queen's University Belfast - Research Portal:
Link to publication record in Queen's University Belfast Research Portal

The Origin of B-type Runaway Stars: Non-LTE Abundances as a Diagnostic

Catherine M. McEvoy[1,2,3], Philip L. Dufton[1], Jonathan V. Smoker[1,2], David L. Lambert[4], Francis P. Keenan[1],
Fabian R. N. Schneider[5], and Willem-Jan de Wit[2]

[1] Astrophysics Research Centre, School of Mathematics and Physics, Queen's University Belfast, Belfast BT7 1NN, UK
[2] European Southern Observatory, Alonso de Cordova 3107, Casilla 19001, Vitacura, Santiago 19, Chile
[3] Graduate School, King's College London, The Strand, London SE1 9NH, UK
[4] The University of Texas at Austin, Department of Astronomy, RLM 16.316, Austin, TX 78712, USA
[5] Department of Physics, University of Oxford, Denys Wilkinson Building, Keble Road, Oxford OX1 3RH, UK

Abstract

There are two accepted mechanisms to explain the origin of runaway OB-type stars: the binary supernova (SN) scenario and the cluster ejection scenario. In the former, an SN explosion within a close binary ejects the secondary star, while in the latter close multibody interactions in a dense cluster cause one or more of the stars to be ejected from the region at high velocity. Both mechanisms have the potential to affect the surface composition of the runaway star. TLUSTY non-LTE model atmosphere calculations have been used to determine the atmospheric parameters and the C, N, Mg, and Si abundances for a sample of B-type runaways. These same analytical tools were used by Hunter et al. for their analysis of 50 B-type open-cluster Galactic stars (i.e., nonrunaways). Effective temperatures were deduced using the Si-ionization balance technique, surface gravities from Balmer line profiles, and microturbulent velocities derived using the Si spectrum. The runaways show no obvious abundance anomalies when compared with stars in the open clusters. The runaways do show a spread in composition that almost certainly reflects the Galactic abundance gradient and a range in the birthplaces of the runaways in the Galactic disk. Since the observed Galactic abundance gradients of C, N, Mg, and Si are of a similar magnitude, the abundance ratios (e.g., N/Mg) are as obtained essentially uniform across the sample.

Key words: stars: atmospheres – stars: early-type – stars: rotation – stars: kinematics and dynamics

1. Introduction

The presence of a significant number of early-type OB main-sequence stars in the Galactic halo, as demonstrated by Greenstein & Sargent (1974), has occasioned an extensive literature on the origins of massive young stars far from the Galactic disk, the richest site of star-forming regions. Very broadly, two explanations for halo OB main-sequence stars have survived scrutiny; both explanations consider that the stars formed in the Galactic disk and were ejected from their parental open cluster or association with suffcent velocity to reach the Galactic halo. According to these explanations, the stars deserve their common classification as "runaway" stars. A less likely explanation not considered further here is that the halo OB main-sequence stars were formed in situ (Dyson & Hartquist 1983).

Two proposed scenarios are considered to be capable of producing runaway stars: the binary supernova (SN) scenario (here, BSS) and the cluster ejection scenario (here, CES):

1. In the BSS proposed first by Zwicky (1957) and developed by Blaauw (1961), the runaway star was the secondary in a binary with a more massive star that experienced its terminal SN explosion. The reduced gravitational attraction of the primary's stellar remnant, either a neutron star (NS) or a black hole (BH), freed the secondary to escape with a velocity similar to its orbital velocity. The escaping secondary—the runaway star—may be accompanied by the stellar remnant.
2. In the CES proposed by Poveda et al. (1967), close encounters in a young open cluster may lead to the ejection of a star. Multibody interactions are favored to eject a single or a binary star. Simulations suggest that the most effective way to produce high-velocity runaway

stars is through the interaction of two hard binary systems (Hoffer 1983). Leonard (1989) and Leonard & Fahlman (1991) show that binary–binary interactions may result in runaway single, binary, or even merged binary stars.

As might be expected, both the BSS and the CES contribute to the runaway population. Hoogerwerf et al. (2001—see also de Zeeuw et al. 2001) use astrometric data to predict the past tracks of stars in the Galaxy to show that specific examples of runaways may be attributed to the BSS (see ζ Oph and pulsar PSR J1392+1059) or to the CES (AE Aur and μ Col ejected from Orion—see Blaauw & Morgan (1954) and Gies & Bolton (1986)). Across their sample of runaways, Hoogerwerf et al. (2001) estimate that two thirds arise from the BSS and one third arises from the CES. Other authors consider the CES to be the greater contributor of runaway stars.

In this paper, we provide a non-LTE analysis of C, N, Mg, and Si abundances for a sample of runaway B stars and search for abundance differences among the sample and between the sample and B stars in young open clusters in the Galactic disk. The goal is to determine if the abundance information provides convincing evidence or even intriguing clues to the origin of a runaway. The suggestion to exploit chemical composition to judge the competing origins of runaway stars is traceable to Blaauw (1993), who proposed a study of the He/H abundance versus the projected rotational velocity $v \sin i$ with He enrichment and a high $v \sin i$ resulting from the BSS. He enrichment should generally be accompanied by N enrichment and a parallel C deficiency as a result of H-burning by the CNO cycles. A Mg and Si enrichment of the runaway star may result for stars provided by the BSS but not those provided by the CES. Many previous studies have reported LTE abundance analyses generally giving abundances relative to Galactic disk

Table 1
Each Star Listed by HIP Number, Along with an Alternative Identifier

HIP	Other	Vmag	Spec. Type	Obs.[a]	v_r km s^{-1}	$v \sin i$ km s^{-1}	Reference[b]
2702	HD 3175	9.33	B4V	F	-13 ± 2	26 ± 2	S11
3812	CD -56 152	10.18	B2V	U	14 ± 8	194 ± 7	S11
7873	HD 10747	8.15	B2V	F	-9 ± 2	15 ± 1	T11
13489	HD 18100	8.44	B5II/III	F	80 ± 7	241 ± 6	M05
16758	HD 22586	9.33	B4V	F	-13 ± 2	88 ± 3	S11
45563	HD 78584	8.20	B3	T	-120 ± 6	102 ± 4	T11
55051	HD 97991	7.41	B2/3V	U	31 ± 3	135 ± 3	S11
56322	HD 100340	10.12	B0	T, U	253 ± 10	181 ± 10	S11
60615	BD $+36$ 2268	10.31	B3V	T	31 ± 4	54 ± 4	S11
61431	HD 109399	7.67	B0.5III	F	-43 ± 3	203 ± 6	T11
64458	HD 114569	8.10	B7/8	F	104 ± 2	74 ± 1	M12
67060	HD 119608	7.53	B1Ib	F	31 ± 1	59 ± 9	M04
68297	HD 121968	10.26	B1V	T, U	17 ± 9	199 ± 27	S11
70205	LP 857-24	11.36	⋯	F	243 ± 4	64 ± 4	B12
70275	HD 125924	9.66	B2IV	T	244 ± 1	64 ± 3	S11
79649	HD 146813	9.06	B1.5	T	21 ± 2	87 ± 3	S11
81153	HD 149363	7.81	B0.5III	F, T, U	145 ± 3	88 ± 10	S11
85729	HD 158243	8.15	B1Ib	F	-63 ± 2	70 ± 2	M12
91049	HD 171871	7.78	B2IIp	T	-64 ± 1	44 ± 1	T11
92152	HD 173502	9.70	B1II	F	49 ± 1	53 ± 3	K82
94407	HD 179407	9.44	B0.5Ib	F	-120 ± 4	134 ± 9	S97
96130	HD 183899	9.93	B2III	F	-46 ± 2	55 ± 3	S11, T11
98136	HD 188618	9.38	B2II	F	46 ± 4	167 ± 3	S11
101328	HD 195455	9.20	B0.5III	F, U	19 ± 7	213 ± 7	S11
105912	HD 204076	8.73	B1V	F, U	0 ± 3	102 ± 1	S11, T11
107027	HD 206144	9.34	B2II	F, U	122 ± 5	184 ± 12	S11
109051	HD 209684	9.94	B2/3III	U	82 ± 2	108 ± 3	S11, T11
111563	HD 214080	6.93	B1/2Ib	F	16 ± 2	108 ± 3	S11
112022	HD 214930	7.40	B2IV	T	-60 ± 4	12 ± 1	M05
112482	HD 215733	7.34	B1II	T	-6 ± 6	72 ± 1	T11
113735	HD 217505	9.13	B2III/IV	F	-17 ± 1	26 ± 2	S11
114690	HD 219188	7.06	B0.5III	F, T	73 ± 19	239 ± 15	S11
115347	HD 220172	7.64	B3Vn	F	26 ± 2	39 ± 1	S11
115729	HD 220787	8.29	B3III	F	26 ± 2	26 ± 2	S11, T11
⋯	EC 05582-5816	9.46	B3V	F	85 ± 13	221 ± 5	S11
⋯	EC 13139-1851	10.50	B4	U	15 ± 4	43 ± 1	S11
⋯	EC 20140-6935	8.83	B2V	F	-24 ± 2	45 ± 2	S11
⋯	PB 5418	11.35	B2	U	147 ± 3	50 ± 1	S11
⋯	PHL 159	10.90	B	U	87 ± 2	30 ± 1	S11

Notes. Column heads are the *V* magnitudes, the spectral types, the instrument used for observation, the radial velocity, the projected rotational velocity, and the reference that identifies the star as a runaway.

[a] Spectrograph used for the observation: F—Feros, T—Tull, and U—UVES.

[b] References: S11—Silva & Napiwotzki (2011), T11—Tetzlaff et al. (2011), M05—Mdzinarishvili & Chargeishvili (2005), M12—McDonald et al. (2012), M04—Martin (2004), B12—de Bruijne & Eilers (2012), K82—Keenan et al. (1982), and S97—Smartt et al. (1997).

B stars of the same atmospheric parameters—see, for example, the runaway sample analyzed by Martin (2004). This is the first non-LTE analysis of a sample of runaway B stars.

In Section 2, we discuss the selection criteria used to isolate our sample of runaway stars whose spectra were obtained (see Section 3) and analyzed in Section 4 following the method previously applied by Hunter et al. (2009—see also Trundle et al. 2007) to B stars in the three Galactic open clusters. Abundances in the runaway and cluster B stars are discussed in Section 5. Rotational and radial velocities are discussed in Section 6. Brief concluding remarks are offered in Section 7.

2. Selection of Runaway B Stars

Targets were selected from catalogs of previously identified runaway candidates. Different criteria are outlined in each

source identified in the reference column of Table 1 and cited in the footnotes to the table. The table lists the stars by their HIP number where available and/or an alternative designation, the *V* magnitude, the spectral type, the source of our spectra (see the next section), the radial velocity (v_r), the projected rotational velocity ($v \sin i$), and the reference to the star's selection as a runaway B star. All objects in our sample either lie far from the Galactic plane with a height above or below the plane (*z* distance) of >0.3 kpc or have a high Galactic latitude ($|b| > 30°$) or a peculiar space velocity of $\gtrsim 30$ km s^{-1}. A star that meets any one of these criteria is considered a runaway. Essentially each star in our sample has been shown by one or more of the references to have been ejected from the disk, i.e., the travel time from disk to its halo location is less than the lifetime of the star. In the BSS it is expected that the ejection

velocity gained from the loss of mass from the binary system as a result of the SN will not exceed 300–400 km s^{-1}, while for the CES similar velocities are possible (see Leonard 1993; Portegies Zwart 2000; Gvaramadze et al. 2009). A majority of the runaway stars are expected to be bound to the Galaxy. Stars exceeding the escape velocity are generally called "hypervelocity" stars, and the principal ejection engine for such stars is the Galaxy's central supermassive black hole (see review by Brown 2015). Two hypervelocity stars originating in the outer Galaxy are known: HD 271791 (Heber et al. 2008; Przybilla et al. 2008) and HIP 60350 (Irrgang et al. 2010). Such stars may be products of the BSS operating in a binary that has particular initial masses.

One of our two primary sources of runaway B stars is a list by Silva & Napiwotzki (2011) of 174 high-Galactic-latitude B stars drawn from the literature. As noted by Silva & Napiwotzki and emphasized by essentially all previous discussion of runaway B stars, the spectral classification of B type does not ensure that the star is a B main-sequence (massive) star because low-mass stars evolving either off the blue horizontal branch or from the asymptotic branch stars (i.e., post-AGB stars) can encroach on the effective temperature— surface gravity (T_{eff}, log g) plane occupied by main-sequence B stars—see also Tobin (1987). Using then-available information on (T_{eff}, log g) and data on atmospheric abundances, Silva & Napiwotzki identified which of the 174 stars belong or possibly belong to the main sequence (MS or MS?). With one exception, the stars we observed from Silva & Napiwotzki's Tables 2 and 3 were classified as MS or MS? The one exception was HIP 60615 (BD +36 2268), which was classified as non-MS. As massive stars, the combination of effective temperature and surface gravity indicate that the sample spans the mass range of about 5–25 solar masses. The estimated ejection velocities range up to about 400 km s^{-1} (Silva & Napiwotzki 2011) and do not lead to escape from the Galaxy. The actual space velocities of observed runaways are smaller than the ejection velocities because stars are generally observed near the apex of their orbit where they spend most of their time.

Our second primary source of runaway B stars is the catalog of young runaway stars within 3 kpc of the Sun compiled by Tetzlaff et al. (2011) using *Hipparcos* astrometry. We selected 13 B stars from this catalog of more than 2500 stars younger than about 50 My and with peculiar velocities; of these, six also belong to our selection from Silva & Napiwotzki (2011).

Our sample was completed by selecting another 10 targets from the literature on runaway stars.

3. Observations

High-resolution high signal-to-noise optical spectra were collected from three telescopes over a period of 16 months. The wavelength coverage and observation dates of each data set are shown in Table 2. Each set of observations is described below, along with the reduction procedures through which they were prepared for analysis.

3.1. FEROS Observations

Twenty-six targets were observed in 2014 August, using the ESO FEROS instrument (Kaufer et al. 1999), a high-resolution ($R \approx 48,000$) prism cross-dispersed echelle spectrograph. FEROS has almost complete spectral coverage from 3500 to 9200 Å and provides a high S/N (≈ 300—see Table 2) in

Table 2
Observation Dates and Wavelength Coverage of Each Instrument

Instrument	λ Coverage (Å)	Dates
FEROS	3500–9200	2013 Aug
Tull	3400–10900	2013 May/Jun
UVES blue arm	3730–4990	2014 Mar–Jul
UVES red arm	5650–9460	2014 Mar–Jul

relatively short exposure times for bright stars. All data were reduced using the ESO FEROS pipeline (version 1.57). Multiple exposures were combined using either a median or a weighted average, within IRAF.[6] Both these methods of merging the exposures resulted in very similar spectra, with the weighted average giving a slightly higher signal-to-noise ratio, and so these were adopted. Occasionally cosmic ray events were visible, but these were easily removed from the spectra manually, if they interfered with any analysis.

Four targets (HD 1999, HD 165955, HD 204076, and HD 208213) were deemed unusable for abundance analysis. HD 1999 showed double lines in its spectrum, making quantitative analysis unreliable. HD 165955 has a very high $v \sin i$, so many lines became unobservable. HD 204076 proved to be a double-lined spectroscopic binary when it was observed with UVES. HD 208213 did not have a sufficient S/N to identify the Si III lines required for our analysis. It was also observed with UVES and discarded for the same reason.

3.2. UVES Observations

Seventeen targets were observed at the Very Large Telescope using the UVES instrument (Dekker et al. 2000), a high-resolution ($R \approx 80,000$), high-efficiency, cross-dispersed echelle spectrograph with a blue arm and a red arm. A standard setting (437+760) was used, yielding a wavelength coverage of 3730–4990 Å in the blue arm and 5650–9460 Å in the red arm. All of the data were taken directly from the ESO archive, having been reduced using the ESO UVES pipeline (Ballester et al. 2000). Multiple exposures were normalized and combined using either a median or a weighted σ-clipping algorithm, within IDL. As the S/N of the individual exposures was high, the final spectra from both methods were effectively indistinguishable. Again, any cosmic ray events that interfered with subsequent analysis were removed manually.

As the UVES data set was obtained to extend our study to a higher $v \sin i$ and fainter targets, some of these proved particularly difficult to analyze and five were discarded, leaving 12 for which atmospheric parameters and abundances have been estimated.

3.3. McDonald Observations

Fourteen runaway candidates were observed at the W. J. McDonald Observatory with the Tull coudé echelle spectrograph at the 2.7 m Harlan Smith telescope (Tull et al. 1995), with a high spectral resolution ($R \approx 60,000$), during 2013 May and June. Spectra were obtained covering a wavelength range of 3400–10900 Å. The echelle data were

---

[6] IRAF is distributed by the National Optical Astronomy Observatory, which is operated by the Association of Universities for Research in Astronomy under cooperative agreement with the National Science Foundation.

split into orders, each of which was reduced separately using standard IRAF procedures.

For stars with significant rotational broadening and/or large surface gravities, the Hδ line profiles extended over a significant fraction of the order. Therefore, the normalization of these data proved more difficult than the normalization of those from UVES and FEROS. To deal with this concern, blaze fits were made to the bracketing orders, where the continuum was obvious, and these were averaged to provide a blaze profile for the order containing Hδ. This was then used to rectify the orders containing Hδ. All data were subsequently normalized and multiple exposures combined using either a median or a weighted σ-clipping algorithm, within IDL, as with the UVES observations discussed above.

Three of the McDonald targets were not analyzed. HD 69686 and HD 118246 did not have a sufficient S/N to identify the rotationally broadened Si III lines, preventing estimates of the projected rotational velocities, effective temperatures, and microturbulences. HD 203664 had complex and variable spectra (Aerts et al. 2006) and so was removed from the sample.

4. Method of Analysis

Non-LTE model atmosphere grids and model atoms from the TLUSTY and SYNSPEC codes (Hubeny 1988; Hubeny & Lanz 1995; Hubeny et al. 1998; Lanz & Hubeny 2007) were used to derive atmospheric parameters and chemical abundances. More detailed discussions of our analysis methods can be found in Hunter et al. (2007), while those of the atmospheric grids are in Ryans et al. (2003) and Dufton et al. (2005).[7] Hence only a brief summary is given here.

Model atmosphere grids have been generated with metallicities representative of the Galaxy ([log (Fe/H) + 12] = 7.5 dex, and other abundances scaled accordingly). These model atmospheres cover a range of effective temperatures from 12,000 to 35,000 K in steps of 500–1500 K, and surface gravities ranging from close to the Eddington limit to 4.5 dex in steps of 0.15 dex (Hunter et al. 2008).

The codes make non-LTE assumptions, i.e., the atmospheres can be considered plane parallel with winds having no significant effect on the optical spectrum, and a normal He-H ratio (0.1 by number of atoms) is assumed. Dufton et al. (2005) and McEvoy et al. (2015) independently tested the validity of this approach. They analyzed the spectra of B-type supergiants in the SMC and the LMC, respectively, using the grids described here and also the FASTWIND code (Santolaya-Rey et al. 1997; Puls et al. 2005), which incorporates wind effects. Dufton et al. (2005) found excellent agreement in the atmospheric parameters estimated from the two methods. The effective temperature, logarithmic surface gravity, and micro-turbulent velocity estimates all agreed to well within their errors. The abundance values agreed to within 0.1 dex for elements such as C, O, Si, and Mg, while the discrepancies in N abundances were less than 0.2 dex, although a systematic difference of ~0.1 dex did appear to exist between the two approaches. Dufton et al. (2005) suggested that this was due to differences in the N model atoms and the wind effects adopted. McEvoy et al. (2015) also found good agreement between results from the two codes. Of the 11 stars analyzed using both methods, five targets had effectively identical results and five

agreed well (with differences $\leqslant$1000 K in $T_{\rm eff}$, $\leqslant$0.1 dex in log g, and $\leqslant$0.2 dex in N abundance estimates), with the N abundance in only one target showing significant discrepancies between the methods. However, this star is an extreme object, close to the Eddington limit, where N abundances will be less secure. As the majority of our sample is lower-luminosity dwarfs or giants, our approach should be adequate.

We adopt baseline chemical abundances from Hunter et al. (2007, 2009) derived from a sample of B-type stars in the Milky Way. Other B-type stellar studies, such as those by Lyubimkov et al. (2005, 2013), Daflon et al. (2009), Simón-Díaz et al. (2010), and Nieva & Simón-Díaz (2011), have found higher baseline abundances for Mg, Si, and N, closer to Solar abundances, but to maintain consistency in our analysis we use the Hunter baseline values that for N, Si, and Mg are 7.62, 7.42, and 7.25 dex, respectively (see Hunter et al. 2007, 2009).

It is important to note that the stellar metallicity distribution in a disk galaxy, including the Milky Way, typically exhibits a negative gradient as a function of distance from the Galactic center, in both the radial and the vertical directions (Huang et al. 2015). Examples of studies where radial N abundance gradients in the Galactic disk have been studied include Rolleston et al. (2000), who found a gradient of -0.09 ± 0.01 dex kpc^{-1}, while Daflon & Cunha (2004) found an average gradient for all elements in the Galactic disk of -0.042 ± 0.007 dex kpc^{-1}, with an N value of -0.046 ± 0.011 dex kpc^{-1}, half of that estimated by Rolleston et al. (2000). Both of these measurements rely on abundances in young OB-type stars. Shaver et al. (1983) used radio and optical spectroscopy to sample Galactic H II regions, spanning 3.5–13.7 kpc from the Galactic center. They found a N abundance gradient of -0.09 ± 0.015 dex kpc^{-1}, similar to Rolleston et al. (2000), along with evidence of steeper gradients in the inner regions of the Galactic disk. Huang et al. (2015) investigated this effect both radially and vertically using 7000 red clump stars between 7 and 14 kpc from the Galactic center. They found that between 7 and 11.5 kpc the radial gradient flattens as the height from the Galactic plane increases, but that between 11.5 and 14 kpc the gradients do not vary with height and are at a constant value of -0.014 dex kpc^{-1}. Rolleston et al. (2000) also considered a two-zone model but found no evidence to indicate that this was more appropriate. Here, an average N abundance for Galactic B-type stars has been adopted from Hunter et al. (2009), although this value may be slightly higher if stars were formed closer to the Galactic center and lower if they were formed far from it. However, in no case has the gradient been found to be very large, so the metallicity distribution should not have a significant effect on the results presented here.

4.1. Atmospheric Parameters

The three characteristic parameters of a static stellar atmosphere (effective temperature, surface gravity, and micro-turbulence) are interdependent, so an iterative process was used to estimate these values (see Fraser et al. 2010; McEvoy et al. 2015 for more details). The parameters are described separately in the subsections below. The final values for these parameters are given in Table 3.

4.1.1. Effective Temperature

Effective temperature ($T_{\rm eff}$) estimates were determined using the Si ionization balance. Equivalent widths of the Si III

---

[7] See also http://star.pst.qub.ac.uk.

Table 3
Final Atmospheric Parameters for Each Star, Listed by HIP Number, with Another Identifier Shown[a]

HIP	Other	$T_{\rm eff}$ K	$\log g$ cm s^{-2}	$v_{\rm t}$ km s^{-1}	Mg	Si	N	C
2702	HD 3175	16100	3.6	8	6.85	7.02	7.35	7.82
3812	CD −56 152	17000	3.4	14	6.83	6.83	7.42	⋯
7873	HD 10747	18700	3.8	8	7.03	7.01	7.33	7.69
13489	HD 18100	23500	3.6	15	7.05	6.64	7.42	⋯
16758	HD 22586	21700	3.3	14	7.44	7.62	7.93	8.13
45563	HD 78584	18600	3.8	8	7.01	6.81	7.31	⋯
55051	HD 97991	21500	3.8	5	6.98	7.36	7.58	⋯
56322	HD 100340	24500	3.8	4	7.43	7.55	7.61	⋯
60615	BD +36 2268	19600	3.4	9	6.97	6.82	7.66	⋯
61431	HD 109399	23000	3.1	16	7.38	7.24	7.42	⋯
64458	HD 114569	18300	3.8	6	7.21	7.24	7.90	8.39
67060	HD 119608	19900	2.7	16	7.52	7.67	7.93	8.05
68297	HD 121968	20550	3.4	0	7.43	7.98	7.72	⋯
70205	LP 857-24	24600	4.1	0	7.45	7.46	7.42	⋯
70275	HD 125924	21000	3.6	6	7.08	7.13	7.28	⋯
79649	HD 146813	19400	3.2	5	7.02	7.25	7.47	⋯
81153	HD 149363	27800	3.5	12	7.60	7.79	7.86	8.22
85729	HD 158243	19300	2.7	20	7.37	7.69	7.91	8.02
91049	HD 171871	20300	3.4	14	7.35	7.51	7.81	⋯
92152	HD 173502	25600	3.5	12	7.51	7.74	7.98	⋯
94407	HD 179407	26000	3.4	17	8.00	7.82	8.21	8.53
96130	HD 183899	20000	3.3	17	7.18	7.53	7.80	7.98
98136	HD 188618	21300	3.4	11	7.32	7.34	7.85	⋯
101328	HD 195455	20550	3.2	14	7.47	7.74	7.96	7.83
105912	HD 204076	20100	3.4	20	7.19	7.43	7.97	⋯
107027	HD 206144	17750	2.5	16	7.24	7.31	7.56	7.68
109051	HD 209684	20340	3.9	9	6.98	7.17	7.54	⋯
111563	HD 214080	19400	2.9	17	7.18	7.63	7.56	7.81
112022	HD 214930	18000	3.4	6	7.04	7.04	7.27	⋯
112482	HD 215733	23100	2.9	14	7.39	7.40	7.60	⋯
113735	HD 217505	21600	3.9	3	7.27	7.33	7.56	7.97
114690	HD 219188	23200	3.0	13	7.37	7.71	7.66	7.86
115347	HD 220172	21700	3.8	0	7.31	7.41	7.69	7.95
115729	HD 220787	18600	3.6	5	7.01	7.07	7.51	7.91
⋯	EC 05582-5816	15900	3.4	10	6.97	7.43	8.40	8.39
⋯	EC 13139-1851	18100	3.9	13	7.09	7.21	7.64	⋯
⋯	EC 20140-6935	21900	3.8	0	7.20	7.47	7.72	8.09
⋯	PB 5418	19300	3.8	8	7.05	7.07	7.44	⋯
⋯	PHL 159	22900	4.1	0	7.46	7.41	7.46	⋯

Notes. The effective temperatures, surface gravities, and microturbulences are given for each star, along with the Mg, Si, N, and C abundances where available.
[a] Analysis of EC 05582-5816 is based on model atmospheres with the Si abundance set to 7.4. For all other analyses, the Si abundance is determined from Si lines and the microturbulence is determined from the Si III lines.

multiplet (4552, 4567, 4574 Å) were measured, together with those for the Si IV lines at 4089 and 4116 Å in the hotter targets and those of Si II at 4128, 4130 Å in the cooler stars. For narrow-lined, high S/N targets, a simple Gaussian profile fit was sufficient to obtain a reliable equivalent width measurement (see Figure 1, upper left plot). The uncertainties in these measurements are typically of the order of 10% (Hunter et al. 2007). For stars with higher projected rotational velocities ($v \sin i \geqslant 50$ km s^{-1}), it was more appropriate to fit rotationally broadened profiles, as rotation becomes the dominant broadening mechanism (see Figure 1, upper right plot). In some cases it was not possible to measure the strength of either the Si II or the Si IV spectrum. For these targets upper limits were set on their equivalent widths, allowing constraints to the effective temperatures to be estimated (see, e.g., Hunter et al. 2007 for more details). This was mostly the case for stars with large projected rotational velocities and midrange temperatures (18,000–26,000 K). The random uncertainty in

our effective temperatures is approximately ±1000 K (about 5%), consistent with the high quality of the observational data. In those cases where upper limits were set for the equivalent widths of the Si absorption lines, the values will obviously be more uncertain and so error bars of ≈2000 K are more appropriate.

4.1.2. Surface Gravity

The logarithmic surface gravity ($\log g$) was estimated by comparing the theoretical and the observed profiles of the hydrogen Balmer line Hδ. Automated procedures were developed to fit the theoretical spectra to the observed lines, with regions of best fit defined using contour maps of $\log g$ against $T_{\rm eff}$. Using the effective temperatures deduced by the methods outlined above, the gravity could be estimated. The effects of instrumental, rotational, and macroturbulent broadening, which have the most significant effect on the line cores,
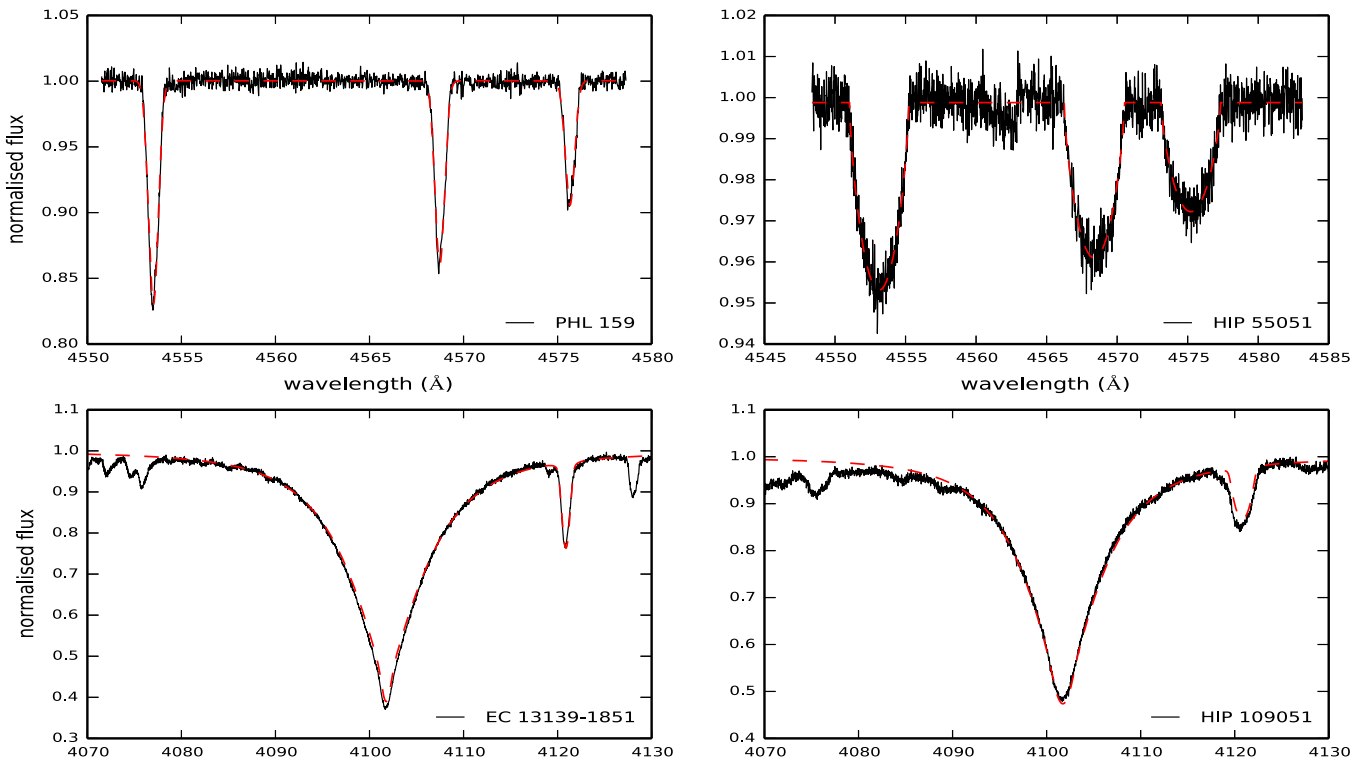
Figure 1. Upper left plot: Si III spectrum for PHL 159 ($v \sin i = 30$ km s^{-1}), with Gaussian model fits (red dotted line) used to determine v_t and $T_{\rm eff}$. Upper right plot: Si III spectrum for HIP 55051 ($v \sin i = 135$ km s^{-1}), with rotationally broadened model fits (red dotted line) used to determine v_t and $T_{\rm eff}$. Lower left plot: H δ spectrum for EC 13139-1851 ($v \sin i = 43$ km s^{-1}), along with its model fit, used to determine $\log g$. Lower right plot: H δ spectrum for HIP 109051 ($v \sin i = 108$ km s^{-1}), along with its model fit, used to determine $\log g$.

were considered in the theoretical profiles (see Figure 1, lower plots). Uncertainties in the fitting procedures led to random errors of ±0.1 dex, while systematic errors could be present due to, e.g., the uncertainty in the adopted line broadening theory or in the model atmosphere assumptions. Additional errors might arise from the uncertainty of the identification of the continuum around Hδ in the McDonald spectra (see Section 3.3), where less continuum was available around the line.

4.1.3. Microturbulence

Following standard practice, we derived the microturbulent velocity from the Si III triplet (4552, 4567, and 4574 Å—see upper plots in Figure 1) as it is observed in all our analyzable spectra and because all three lines arise from the same multiplet, so that errors in the absolute oscillator strengths and non-LTE effects should be minimized.

An alternative approach to the microturbulence determination uses the same Si III triplet but finds the microturbulence that gives the baseline Si abundance of 7.42 from Hunter et al. (2009) as the average from the three lines. This alternative also impacts the determination of the effective temperature and surface gravity and hence the abundances of all elements. In the next section, we comment on the effect on the abundances of the two methods for determining the microturbulence.

4.2. Elemental Abundances

N, Mg, Si, and in some cases C abundances for each star have been estimated using the atmospheric parameters given in Table 3 and measurements of the absorption lines. Abundances are given in Table 3. The atmospheric parameters agree well

between the observations with the different spectrographs. Effective temperatures show differences not larger than 1200 K in all cases, while the range of the logarithmic gravity estimates is only greater than 0.2 dex in one instance (HD 121968 with a range of 0.25 dex). Differences in microturbulence are less than 6 km s^{-1} in all cases. The agreement between atmospheric parameters derived from observations obtained with different instruments is reassuring but not surprising given the high quality of all spectra. This agreement is of course not a measure of any systematic errors.

Extensive appendices in Hunter et al. (2007) show how errors in the atmospheric parameters for B-type stars translate into errors in derived abundances. Hunter et al. (2007) considered the errors to be independent but in reality the situation will be more complicated, as this is not the case. For example, an increase in the effective temperature estimate will lead to an increase in the gravity estimate, and this leads to the theoretical N II equivalent widths (and hence N abundances) being less sensitive to changes in the atmospheric parameters than if these are considered to vary independently.

For the range in atmospheric parameters found for our sample, the simulations of Hunter et al. (2007; see, e.g., their Figure 6 for the N II 3995 Å line) imply that our estimated errors in both the gravity and the microturbulence lead to relatively small errors in the N abundance estimate of 0.1 dex or less. Errors in effective temperature estimates are more important and lead to larger uncertainties with an error of $\Delta T_{\rm eff} \pm 1000$ K translating into an N abundance error of approximately ∓ 0.2 dex at an effective temperature of 18,000 K but decreasing to ~0.1 dex at an effective temperature of 25,000 K. In addition, there will be random errors in the N abundance estimates due to uncertainties in the N II
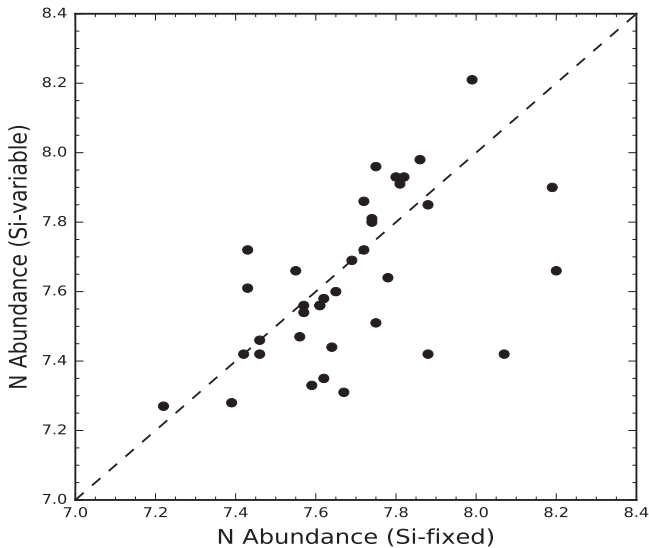
Figure 2. N abundances from models with the microturbulence set by the condition that the Si abundance is 7.40 vs. the N abundances set by the determination of the microturbulence from the Si III lines. The solid line of unit slope corresponds to an abundance independent of the method of fixing the microturbulence.

Figure 3. Spectrum around the N II line at 3995 Å for the most N-enhanced star, EC 05582-5816. HD 78584 is overplotted in red for comparison, as it has a similar spectral type (B3) and a $v \sin i$ of 102 km s^{-1}. Although the N line is heavily broadened in EC 05582-5816, due to its very high $v \sin i$ of 221 km s^{-1}, it can still clearly be seen so it must be particularly strong to avoid being smeared out into the surrounding continuum.

equivalent widths. The latter have been estimated as $\pm 10\%$, which would imply an uncertainty of ~ 0.1 dex. Combining these different sources of error in quadrature would lead to typical uncertainties of 0.2–0.3 dex.

For the atmospheric parameters and abundances in Table 3, the microturbulence was derived from the three Si III lines with the condition that the three lines return the same Si^{2+} abundance. This method was successful for all but EC 05582-5816, for which lines are greatly rotationally broadened. As we noted above, the alternative method is to assume a standard Si abundance of 7.4 for the determination of the microturbulence and hence other atmospheric parameters that finally define the model atmosphere used to determine the abundances of C, N, and Mg. (This alternative method was used by Hunter et al. 2007 in their analysis of B stars in three Galactic clusters.) The C, N, and Mg abundances are little affected by how the microturbulence is chosen; the preferred and alternative methods give similar results. This is well shown by Figure 2, where we show the N abundances obtained when the microturbulence is set by the condition that the Si abundance is 7.4 plotted versus the abundances obtained when the microturbulence comes from the three Si III lines. It is seen that the N abundances are not systematically different in the two cases except for two or three outliers. Obvious outliers are HD 18100 and BD +36 2268 with N abundances obtained from the alternative method of 7.97 and 8.20, respectively. A similar correspondence between abundances from the two methods is found for Mg and for the limited number of determinations of the C abundances. Thus, apart from the artificial constraint of a constant Si abundance, the abundance analyses for all other elements are expected to be largely unaffected by the method used to determine the microturbulence and hence the atmospheric parameters.

For a subsample of our stars (all stars observed with FEROS) we estimated C abundances. The C II line at 4267 Å was used to calculate abundances as it is the only measurable line in all of the spectra. This line is known to be susceptible to (subtle) non-LTE effects (Nieva & Przybilla 2006, 2008), which are not fully taken
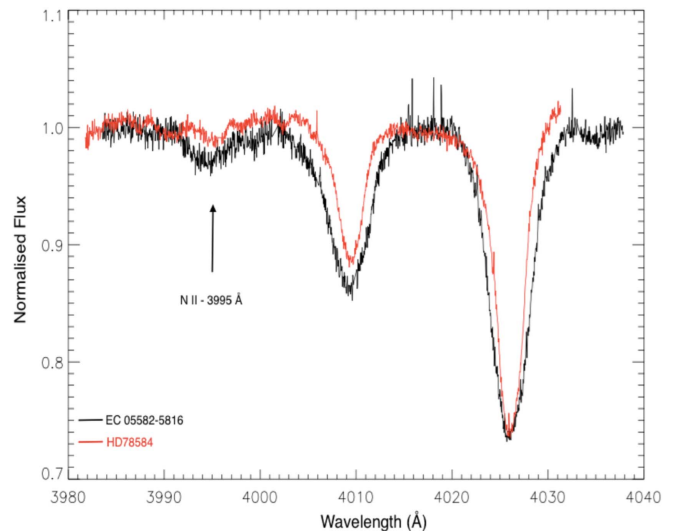
into account in the model ion that was included in the TLUSTY calculations—see discussion by Hunter et al. (2009). Our interpretation of the various abundances is in part referenced to the abundance analysis of Galactic clusters by Hunter et al. (2007), who also exclusively used the 4267 Å line; thus the inability to account fully for the non-LTE effects should be almost canceled by the comparison with the Galactic clusters.

N abundances in Table 3 were estimated from the singlet transition at 3995 Å as it is one of the strongest N II lines in the optical spectrum and appears unblended. Two examples of spectra of high $v \sin i$ stars around the N line at 3995 Å are shown in Figure 3. Other N II lines were also present in a significant number of observations, including those between 4601 and 4643 Å and the singlet at 4447 Å. These tended to be more blended and so may lead to less accurate abundance estimates than those from 3995 Å. It is interesting to note that Lyubimkov et al. (2013) found that the line at 3995 Å gave a lower N abundance in their sample compared with the abundance from other transitions and that the differences were a function of effective temperature, ranging from -0.3 dex at 16,000 K to 0.0 dex at 29,000 K. In our case, the difference is about -0.1 dex over the full temperature range with a rise to 0.0 dex below about 18,000 K. These differences with Lyubimkov et al. (2013) likely reflect differences in the adopted model atoms. By referencing our abundances from the 3995 Å line to those from Hunter et al. (2009), we expect to obtain a true measure of abundance differences between the cluster (i.e., the Galactic disk) and the runaway B stars. Mg abundances were estimated for all spectra using the Mg II transition at 4481 Å, comprising three overlapping lines of a single multiplet.

Si abundances are obtained from the lines of Si II, Si III, and Si IV referred to in the determination of the atmospheric parameters.

5. Ejection Mechanisms and Abundances

The most satisfying discussion of the abundances would conclude with the demonstration that runaway B stars formed

by the BSS and the CES have distinct differences in composition with both scenarios providing abundance differences with B stars in Galactic open clusters. Perhaps the least satisfying result would be one in which the runaway B stars showed a common pattern of abundances and one that matched well the abundances of B stars in Galactic open clusters—i.e., the BSS and CES scenarios both preserve the abundances of the investigated elements. Yet in this case one hopes that the origin of runaway stars may be traced from other observational indicators such as binarity and rotational velocities.

The X-ray sources known as low-mass X-ray binaries (LMXBs) consist of a low-mass "normal" secondary star orbiting a BH or an NS where the SN leading to the BH or NS possibly contaminated the secondary. Abundance analysis of the secondary should offer clues to the contamination expected in the BSS mode of runaway star formation. One LMXB secondary accompanying a BH has a spectral type of B9III and with an effective temperature of 10,500 K approximates a runaway star. With [Fe/H] = 0.0, this secondary in V4641 Sgr has a normal composition (C, O, Mg, Al, Si, and Ti) but an +0.8 dex overabundance for N and Na (Sadakane et al. 2006). Curiously, this star appears to be a replica of EC 05582-5816 (see Section 5.3). Unfortunately C and N abundances have not been reported for the other six LMXB secondaries. The secondary with the most extreme enrichments would appear to be Nova Sco 1994 (González Hernández et al. 2008) with, for example, [Fe/H] = −0.1 but [Mg/Fe] = +0.4 and [Si/Fe] = +0.7 and other anomalies including [O/Fe] = +1.0 and [S/Fe] = +0.9. Mg and Si abundance estimates are available for five secondaries. Comparisons with normal F, G, and K dwarfs are made in the [Fe/H] versus [X/Fe] plane where X = Mg or Si. The mean [Fe/H] for the five stars is +0.1 with a spread from −0.1 to +0.3. The mean difference with respect to normal stars of the same [Fe/H] is [Mg/Fe] and [Si/Fe] at +0.2 with a spread from 0.0 to about +0.7, but the Mg and Si enrichments would be larger if Fe were also enriched. There is a hint that [Mg/Fe] and [Si/Fe] are positively correlated. Other elements considered for four or more of the secondaries but not included in our analysis include the following with mean differences of [X/Fe] relative to normal stars: +0.4 (O), +0.4 (Na), +0.1 (Al), 0.0 (Ca), +0.2 (Ti), and +0.1 (Ni). Again, elemental abundance enrichments are larger if SN Fe contaminates the secondary. Predicted enrichments depend on many factors including uncertain aspects of the SN explosion and do not completely account for the composition of these secondaries. In summary, as far as the elements considered here are concerned the observations of C and N are too few to suggest a pattern but Mg and Si may be enriched simultaneously in some cases.

Possible changes of composition occurring at the birth of a runaway star have to be extracted from the observed composition, bearing in mind that two other factors may affect the chemical composition of the B stars prior to their conversion to a runaway star: first, the initial composition of B (and other) stars depends on the location of their birth site; studies of the composition of stars and H II regions show that abundances decline with increasing distance from the Galactic center. For example, Daflon & Cunha (2004) (regarding B stars) and Luck & Lambert (2011) (regarding Cepheids) find that the abundance gradients for our elements are about −0.045 dex kpc^{-1}, a value representative of many other studies. Azimuthal variations are considered to be smaller than the radial variation. Since runaway stars in the sample catalogs are expected to have birth sites spanning several kpc in the Galactic disk, abundance variations of several 0.1 dex may be anticipated. Second, B stars may be prone to mixing between the surface and the interior, resulting in changes of composition as CN-cycled H-burning products reach the atmosphere—i.e., He/H is increased with a coupled decrease of C and an increase of the N abundance—see, for example, calculations of surface abundances along evolutionary tracks for rotating massive stars by Brott et al. (2011). (Extreme mixing may contaminate the atmosphere with ON-cycled H-burning products, resulting in decreases of O and additional increases of N and He.)

5.1. Mg and Si

Since the Mg and Si abundance should be unaffected by mixing within evolving B stars but could conceivably be altered in runaway stars created by the BSS, we discuss this pair of elements ahead of our discussion of C and N. Our reference Galactic B stars are the three open clusters analyzed by Hunter et al. (2009): NGC 6611, at a Galactocentric distance R_G of 6.1 kpc; NGC 3293, at R_G = 7.6 kpc; and NGC 4755, at R_G = 8.2 kpc, where R_G is taken from Rolleston et al. (2000). (Daflon & Cunha 2004 give somewhat different estimates.) Abundances provided by Hunter et al. (2009) correspond to the atmospheric parameters chosen by assuming an Si abundance of 7.4 (see Section 4 for comments on such a choice). Since the 2.1 kpc difference in Galactocentric distance across the three open clusters should correspond to an abundance difference of only about 0.09 dex, the assumption of constant Si abundance is likely not a source of significant systematic error. The Mg abundances for the three Galactic clusters are just consistent with the anticipated 0.09 dex decline between NGC 6611 and NGC 4755. Of course the Si abundances are not expected to betray the abundance gradient because the condition Si = 7.4 was imposed on the analysis.

For the runaway B stars, the Mg and Si abundances from Table 3 are compared in Figure 4, which shows that Mg and Si abundances are highly correlated and that each range over 1.0 dex. The straight line in Figure 4 corresponds to a constant Mg/Si ratio set at the "standard" ratio of −0.17 dex adopted by Hunter et al. (2009). The spread in Mg abundances among the runaway stars far exceeds the range among stars from an individual open cluster, which is a fair measure of the measurement uncertainties given that stars within a cluster share a common Mg abundance. A major contribution to the Mg and Si abundance spread among the runaway stars surely arises because their birthplaces span quite a range in Galactocentric distances even though present Galactocentric distances may not be that different, a range much greater than the range spanned by the three reference open clusters. Indeed, Galactic orbits calculated by Silva & Napiwotzki (2011) give birthplaces from the Galactic center out to nearly 14 kpc for the sample drawn from their paper. However, plots of the Mg and Si abundances versus the estimated Galactocentric distance of a star's birthplace are too ill defined to confirm the abundance gradients obtained from in situ abundance measurements of young stars and H II regions. All but three of our stars have estimated birthplaces between 4 and 10 kpc. The failure to reproduce the observed abundance gradients may be attributable to uncertainties in the locations of the birthplaces and to the contamination of the stars in the BSS by Mg and Si from the SN.
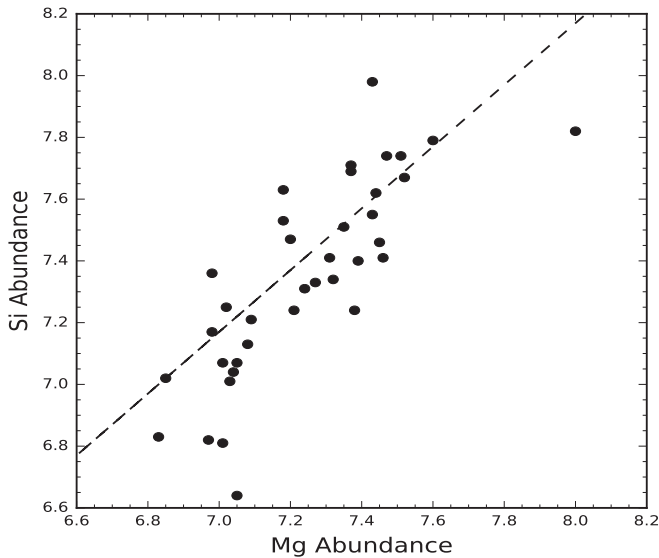
Figure 4. Mg and Si abundances from Table 3. The straight line corresponds to an Mg/Si ratio of −0.17 dex normalized to the standard abundances adopted by Hunter et al. (2009).

Figure 5. C and N abundances plotted for the FEROS sample of runaways. Abundances are taken from Table 3. The straight line, a least-squares fit, shows that the C and N abundances are related over a range of about 1 dex with a scatter consistent with measurement uncertainties—i.e., there are no stars heavily contaminated with CN-cycled products; that is, stars that are C-poor and N-rich. Data for EC 05582-5816 (open circle) are taken from the analysis in which the Si abundance is fixed at 7.4.

Scatter in Figure 4 about the linear relation is consistent with Mg and Si abundance uncertainties and with the spread in Mg abundances within each of the open clusters (see Figure 7, for example). Presence of the linear correlation and a constant Mg/Si ratio are qualitatively expected from the similar nucleosynthetic yields of Mg and Si from SNe II, which are surely the controlling influences on the Galactic abundance gradient whatever the influence of the myriad other factors (e.g., the initial mass function, the star formation rate, Galactic infall etc.) entering recipes for Galactic chemical evolution.

5.2. C and N

Hunter et al. (2009) found that among the B stars in the three reference clusters, the C and N abundances were independent of position on a star's evolutionary track except that half of the few supergiants were enriched in CN-cycled material. Similarly, Lyubimkov et al. (2013) found normal C and N abundances in a sample of 22 slightly evolved B stars (i.e., no supergiants) except for two possibly mixed stars. Thus the expectation is that the majority of the B stars would have preserved their initial C and N abundances before undergoing conversion to a runaway star. The likely corollary of this expectation is that alterations to the C and N abundances may be clues to the process creating the runaway star but that internal CN cycling and mixing to the surface may have occurred independently of formation as a runaway star.

As noted above, the C abundances in Table 3 are provided only for the stars observed with FEROS. Figure 5 shows the C and N abundances for this minority. In Table 3 the C and N abundances for EC 05582-5816, unlike for other stars, are taken from an analysis with the Si abundance fixed at 7.4 but, as noted above, the C and N abundances are expected to be independent of this assumption concerning the Si abundance; the high $v \sin i$ of EC 05582-5816 precluded the use of the Si III multiplet to determine the microturbulence. The C and N abundances are tightly correlated with all stars showing a similar C/N to within the measurement uncertainties. In addition, the three Galactic clusters analyzed by Hunter et al. (2009) have mean C and N abundances falling within the band
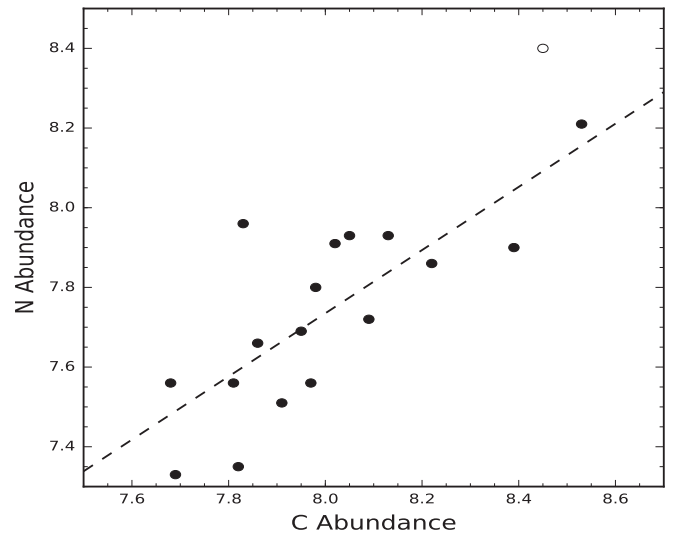
defined by the runaway stars; that is, mean abundances of 8.00 ± 0.19 and 7.62 ± 0.12 for C and N, respectively, for all nonsupergiants in the three Galactic clusters with these abundances provided by analyses assuming that Si has its standard abundance.

These carbon abundances for the subset of our runaway stars show no evidence for a runaway star enriched in CN-cycled material, i.e., a low C abundance paired with a high N abundance such that the total number of C and N atoms is conserved. Very severe contamination with CN-cycled material would result in an N enrichment of up to 0.5–0.6 dex and a severe depletion of C. No such stars are seen in Figure 5. The presence of CN-cycled material may occur in the B star prior to its conversion to a runaway star and is thus not a determining signature of a process resulting in a runaway star.

5.3. N and Mg

To extend the search for abundance anomalies to the complete sample, we examine next the relationship between the N and the Mg abundances. Figure 6, drawing on Table 3, compares the N and the Mg abundances with a distinction made according to surface gravity (i.e., evolutionary status) with stars with log $g < 3.2$ (i.e., supergiants) represented by open circles and stars of higher surface gravity (i.e., main-sequence and slightly evolved stars) represented by filled circles. Figure 7 shows the N and Mg abundances for B stars belonging to the cluster NGC 3293, the best represented of the three clusters studied by Hunter et al. (2009).

With the possible exception of N enrichment from internal mixing or mass loss, one expects the cluster's stars in Figure 7 to share the same N and certainly the same Mg abundance. Thus, the scatter in the N and the Mg abundances in Figure 7 represents the measurement uncertainties that, thanks to the similarity of analytical techniques, will be a very close approximation to the uncertainties affecting the points in Figure 6. (One star—a supergiant—in NGC 3293 appears N-enriched, but this star is not C-depleted.) A comparison of
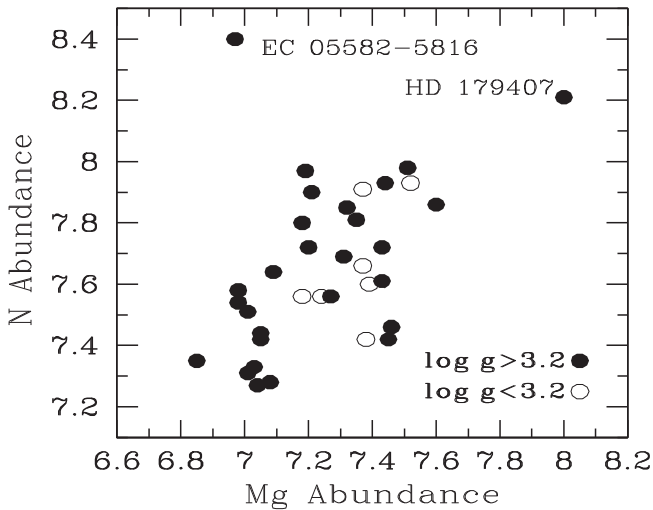
Figure 6. Mg and N abundances from Table 3 with stars distinguished by their surface gravity: log *g* > 3.2, shown as filled circles, and log *g* < 3.2, shown as unfilled circles. Two outliers are identified—EC 05582-5816 and HD 179407—and are discussed in the text.
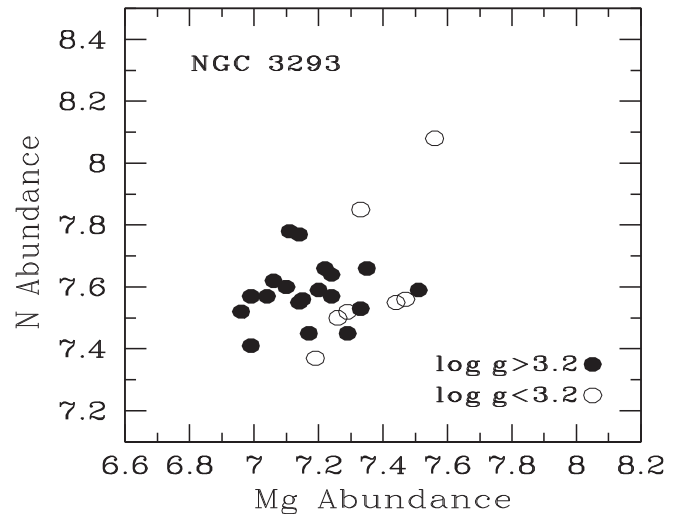

Figure 7. Mg and N abundances for B stars in the open cluster NGC 3293 with data from Hunter et al. (2009). Stars are distinguished by their surface gravity —see caption to Figure 6.

Figures 6 and 7 shows the spread shown by NGC 3293's B stars and hence we conclude that the runaways show an intrinsic star-to-star difference in composition (i.e., C, N, Mg, and Si abundances but with similar abundance ratios), which we attribute to differences in a star's birthplace, with the Galactic abundance gradient being a very likely controlling factor.

EC 05582-5816 and HD 179407 appear as outliers in Figure 6. The two outliers have similar compositions except for their Mg abundances and both appear related to the inner Galaxy. Silva & Napiwotzki (2011) estimate EC 05582-5816's birthplace at 2 pc from the Galactic center. HD 179407 is presently at $R_G = 3.5$ kpc according to Smartt et al. (1997). The pair have very similar C and N abundances (Table 3) but differ substantially in Mg with an abundance of 8.0 for HD 179407 but 7.0 for EC 05582-5816. The Si abundance of HD 179407 is consistent with its Mg abundance. For EC 05582-5816, the present analysis assumes an Si abundance of 7.4. Galactic abundance gradients likely account for the high abundances found for HD 179407. There is a remarkable similarity in composition between EC 05582-5816 and the B9 III secondary of the BH binary V4641 Sgr. This B star has [Fe/H] = 0 and normal abundances of C, O Mg, Al, Si, and Ti but high N and Na overabundances ([N/H] = [Na/H] = +0.8) (Sadakane et al. 2006). If placed in Figure 6, it would provide a third outlier and fall near the two existing outliers. Reobservation and reanalysis of EC 05582-5816, a rapid rotator, is to be encouraged and extended to additional elements.

5.4. Formation Mechanisms and Abundance Anomalies?

N, Mg, and Si abundances across the sampled runaway B stars are similar to those seen in B stars in Galactic clusters. The spread in the C, N, Mg, and Si abundances and the nearly uniform abundance ratios C/N/Mg/Si among runaway stars in our sample results from the combination of two facts: (1) the stars' birthplaces sample a wide range in Galactocentric distances, and (2) the abundances in star-forming regions decline with increasing Galactocentric distance at a rate of approximately 0.05 dex kpc^{-1}. Within our sample there are no

certain outliers with abundance peculiarities. Thus the conclusion is that the two scenarios—BSS and CES—capable of ejecting B (and other) stars from the Galactic disk into the Galactic halo do not as a rule change the surface chemical composition of the runaway star, as sampled by C, N, Mg, and Si. This conclusion from our non-LTE analysis confirms earlier LTE analyses in which the compositions of a runaway star and a comparable B star in the Galactic disk are compared—see, e.g., Martin (2004). Although changes may occur in rare cases, the general conclusion is both disappointing and challenging: disappointing in that the composition, a readily obtainable quantity, appears not to be a discriminant between competing ejection mechanisms; challenging in that other observable quantities now have to been relied on to identify the principal ejection mechanism across a sample of runaway stars and for individual runaway stars. Possible observables include projected rotational velocities and binarity.

6. Ejection Mechanisms: Rotational and Radial Velocities

6.1. Projected Rotational Velocities

The distribution of projected rotational velocities $v \sin i$ for our sample of runaways is very similar to that provided by the B stars in the three Galactic clusters observed by Hunter et al. (2009): velocities up to 300 km s^{-1} with a peak near 50 km s^{-1} and few slow rotators ($v \sin i \leqslant 30$ km s^{-1}). Martin (2006) considered rotational velocities for his sample of runaways and found their frequency distribution to be similar to that assembled by Guthrie (1984) from "young" OB associations whose result is similar to that from the three Galactic clusters. In contrast, B stars in "old" associations and field B stars in the Galactic disk have distributions that rise with a decreasing $v \sin i$ (Wolff et al. 1982; Guthrie 1984). A more recent catalog of projected rotational velocities for 102 northern B stars is provided by Abt et al. (2002).

Tying the $v \sin i$ distribution of the runaways to the ejection mechanisms is unfortunately hampered by the absence of quantitative predictions for the BSS and the CES. In the BSS, if the runaway originates in a close binary system the runaway may be tidally locked, resulting in the rotation velocity being closely related to its orbital velocity. In turn, the ejection

velocity is expected to be related to the orbital velocity. These ideas lead to the expectation that the ejection velocity should be positively correlated with the rotational velocity, but as Martin (2006) demonstrated, runaway stars do not show the expected correlation and therefore the BSS is not the leading producer of runaway stars. For the CES, the likelihood of ejection is plausibly higher in denser environments. On this simple premise and the match between the $v \sin i$ frequency distribution for runaways and young associations, Martin (2006) considered that it seems likely that the [CES] is the dominant mechanism behind his runaway sample and by extension ours too, which has overlap with his sample.

6.2. Radial Velocities

In the BSS, the resulting runaway B star will either be a single B star or form a binary system with a low-mass compact companion (e.g., an NS). A runaway that is single will be paired with a distant ejected NS or a BH moving in a generally opposite direction. Portegies Zwart (2000) suggests that 20%–40% of the runaway B stars should be accompanied by an NS and thus the runaway B star should appear as a single-lined spectroscopic binary with a period of several hundred days.

In the CES, simulations (Leonard & Duncan 1990) suggest that 10% of the runaways will be binaries composed of normal main-sequence stars and likely observable as double-lined spectroscopic binaries.

A definitive test of these predictions for the BSS and the CES will require a radial velocity long-term survey of a large sample of runaway B stars to be put up against more precise predictions about the frequency and nature of the binary populations from the two scenarios. Then, it may be possible to assess in a statistical fashion the relative production rates from the BSS and the CES. For the binaries, it should be possible to assign them to either the BSS (i.e., an NS/pulsar companion) or the CES (i.e., a normal main-sequence companion). For the runaway single stars, the attribution to the formation scenario will be difficult unless one can uncover a subtle abundance anomaly or apply a precise determination of space motions (GAIA)[8] to assist in the identification of the pulsar or the original stellar association.

A definitive observational test is not possible at present. The sole radial velocity survey of high Galactic OB stars was conducted by Gies & Bolton (1986), who concluded that runaway OB stars are deficient in close binaries by a factor of 2–4. Their sample of 15 confirmed runaways provided two binaries (both double-lined systems), and if five probable runways are added, the binary probability becomes 2/20 or 10%. The deficiency of binaries is suggested by reference to the binary fraction of 31% among normal O stars (Garmany et al. 1980) and of 38% among normal B stars (Abt & Levy 1978). Four of our stars (HD 97991, 149363, 214930, and 219188) were in the Gies & Bolton (1986) survey and declared by them to have a constant radial velocity. Martin (2003) found the runaway HD 138503 to be a double-lined spectroscopic binary, a star in Silva & Napiwotzki's (2011) list of runaway stars. HD 1999 and HD 204076, which we observed, are double-lined binaries. Two radio surveys for pulsars reported no detections coincident with runaway OB stars (Philp et al. 1996; Sayer et al. 1996). Unfortunately, the correction for the beaming of pulsar radiation results in an uninteresting limit on the fraction of runaway stars with low-mass compact companions; Sayer et al. (1996) estimate that less than 25%–50% of OB runaways have an NS companion, an (1996) estimate consistent with the prediction by Portegies Zwart (2000).

Our sample can make only a modest contribution to the frequency of binary runaway stars as a test of the BSS and the CES. For the majority of our sample the star was observed once and an assessment of the radial velocity variation must come from velocities reported in the literature. Eight stars were observed at two or more telescopes and thus at different epochs, and the two or three radial velocity measurements may be intercompared and also checked against the literature. (This restricted search for velocity variations is akin to that reported by Martin (2006), who observed many runaway stars at least twice over a few days and also checked velocities against the literature.) We have defined a star with a radial velocity variation between measurements of greater than $20 \, \mathrm{km \, s^{-1}}$ as a possible member of a binary system. This cutoff is set by an inspection of other studies of OB stars (Sana et al. 2013; Dunstall et al. 2015). In some stars, significant velocity variations arise from pulsations, which complicates the search for orbital radial velocity variations, and if neglected as a source of radial velocity variations, the fraction of spectroscopic binaries is overestimated.

Radial velocities are provided in Table 4. Of the eight stars observed twice or thrice by us, seven appear to have a constant velocity. The star with a variable radial velocity is HD 204076, which is certainly a spectroscopic binary; the UVES but not the FEROS spectrum showed double lines. HD 219188 is possibly a variable. There is a $25 \, \mathrm{km \, s^{-1}}$ difference between our two measurements, and online catalogs give a velocity that is either close to the mean of our two or a less positive velocity: $84 \, \mathrm{km \, s^{-1}}$ according to Silva & Napiwotzki (2011) or $64 \, \mathrm{km \, s^{-1}}$ according to Gontcharov (2006) and Kharchenko et al. (2007).

Inspection of Table 4 suggests that four stars observed once by us may be binaries because of a difference with radial velocities reported in the literature. EC 20140-6935 (HD 192273) was noted as a possible binary by Magee et al. (1998), who found a $45 \, \mathrm{km \, s^{-1}}$ velocity difference between their measurement and that reported by Rolleston et al. (1997). Silva & Napiwotzki (2011) gave the velocity as $+17 \, \mathrm{km \, s^{-1}}$ from Rolleston et al. (1997). Our velocity is in good agreement with that by Magee et al. (1998) HD 188618 was suspected by Martin (2006) to be a binary from the velocity difference between his measurement of $29 \pm 6 \, \mathrm{km \, s^{-1}}$ and a previous measurement of $-15 \, \mathrm{km \, s^{-1}}$ by Duflot et al. (1998). Our $-46 \, \mathrm{km \, s^{-1}}$ extends the velocity range. HD 179407's present and previous velocity measurements barely satisfy our $20 \, \mathrm{km \, s^{-1}}$ condition. HIP 70205 (LP 857-24) exhibits a $300 \, \mathrm{km \, s^{-1}}$ difference but the only previous measurement is from the RAVE survey (Kordopatis et al. 2013), which is possibly ill suited to velocity measurements of B stars that provide few lines in the RAVE bandpass. Obviously, this star deserves further attention. Finally there is HD 114569, which has no previous velocity measurement.

It seems fair to conclude that our sample contains few spectroscopic binaries and certainly fewer than the approximately 30% provided by a sample of field B stars in the Galactic disk (Abt & Levy 1978). Our sample is very slightly biased by the exclusion of known double-lined or even single-lined spectroscopic binaries. HD 1999 and the double-lined

---

Table 4
Each Star Listed by HIP Number Along with Alternative Identifier, Radial Velocity from Our Analysis
and from the Literature (with References), and Binary Status of the Star

HIP	Other	Radial Velocity Us[a]	Radial Velocity Literature	Reference[b]	Status
2702	HD 3175	-13 ± 2 (F)	-16 ± 3	R3	Single
3812	CD -56 152	14 ± 8 (U)	19 ± 10	R2	Single
7873	HD 10747	-9 ± 2 (F)	-12 ± 2	R1	Single
13489	HD 18100	80 ± 7 (F)	76 ± 3	R1	Single
16758	HD 22586	99 ± 1 (F)	97 ± 2	R3	Single
45563	HD 78584	-120 ± 6 (T)	-125 ± 2	R1	Single
55051	HD 97991	31 ± 3 (U)	26 ± 3	R3	Single
56322	HD 100340	253 ± 10 (T), 263 ± 4 (U)	254 ± 9	R2	Single
60615	BD $+36$ 2268	31 ± 4 (T)	31 ± 7	R3	Single
61431	HD 109399	-43 ± 3 (F)	-49 ± 2	R1	Single
64458	HD 114569	104 ± 2 (F)	...		Unknown
67060	HD 119608	31 ± 1 (F)	26 ± 4	R1	Single
68297	HD 121968	17 ± 9 (T), 29 ± 3 (U)	28 ± 2	R4	Single
70205	LP 857-24	243 ± 4 (F)	-54 ± 2	R5	Binary?
70275	HD 125924	244 ± 1 (T)	239 ± 2	R4	Single
79649	HD 146813	21 ± 2 (T)	19 ± 6	R4	Single
81153	HD 149363	145 ± 3 (T), 146 ± 3 (U), 144 ± 3 (F)	141 ± 2	R1	Single
85729	HD 158243	-63 ± 2 (F)	-64 ± 3	R1	Single
91049	HD 171871	-64 ± 1 (T)	-62 ± 5	R1	Single
92152	HD 173502	49 ± 1 (F)	68 ± 4	R1	Single?
94407	HD 179407	-120 ± 4 (F)	-119 ± 5	R6	Single
96130	HD 183899	-46 ± 2 (F)	-45 ± 5	R1	Single
98136	HD 188618	46 ± 4 (F)	-15 ± 5	R1	Binary?[c]
101328	HD 195455	19 ± 7 (F), 10 ± 6 (U)	10 ± 6	R3	Single
105912	HD 204076	0 ± 3 (F), 14 ± 2 (U)	-17 ± 7	R2	Binary
107027	HD 206144	122 ± 5 (F), 121 ± 2 (U)	117 ± 8	R4	Single
109051	HD 209684	82 ± 2 (U)	72 ± 8	R4	Single
111563	HD 214080	16 ± 2 (F)	12 ± 4	R6	Single
112022	HD 214930	-60 ± 4 (T)	-63 ± 2	R3	Single
112482	HD 215733	-6 ± 6 (T)	-15 ± 2	R3	Single
113735	HD 217505	-17 ± 1 (F)	-31 ± 10	R2	Single
114690	HD 219188	73 ± 19 (F), 98 ± 19 (T)	64 ± 3	R1	Single?[d]
115347	HD 220172	26 ± 2 (F)	29 ± 3	R6	Single
115729	HD 220787	26 ± 2 (F)	26 ± 3	R4	Single[e]
...	EC 05582-5816	85 ± 13 (F)	81 ± 10	R2	Single
...	EC 13139-1851	15 ± 4 (F)	23 ± 10	R2	Single
...	EC 20140-6935	-24 ± 2 (U)	17 ± 10	R2	Binary[f]
...	PB 5418	147 ± 3 (U)	152 ± 10	R2	Single
...	PHL 159	87 ± 2 (U)	88 ± 3	R2	Single

Notes.
[a] Spectrograph used for the observation: F—Feros, T—Tull, and U—UVES.
[b] References: R1—Gontcharov (2006), R2—Silva & Napiwotzki (2011), R3—Kharchenko et al. (2004), R4—Martin (2006), R5—Kordopatis et al. (2013), R6—Kilkenny & Hill (1975).
[c] Martin (2006) obtained the velocity 29 ± 6 km s^{-1} and also quoted -15 km s^{-1} from Duflot et al. (1998).
[d] R2 gives the velocity as 84 km s^{-1}.
[e] R4 also gives velocities of 24.9 ± 1.5 km s^{-1} from Barbier-Brossat & Figon (2000) and 26.5 ± 2.4 km s^{-1} from Behr (2003).
[f] See Section 6.2.

eclipsing star HD 138503 (Martin 2003) are the only binary stars observed, but they are not in Table 4. With the present understanding of the formation of single and double runaway stars by the BSS and the CES, it is not possible to interpret the low fraction of spectroscopic binaries as a pointer to the more important formation mechanism.

7. Concluding Remarks

Our sample of runaway stars is dominated by B stars that have been ejected from sites of recent star formation in the Galactic disk. Our non-LTE analysis of their C, N, Mg, and Si abundances and published analyses of these elemental abundances by the same non-LTE procedures in B stars in three open clusters in the Galactic disk show no abundance anomalies among the runaways that may be attributed to either of the leading two mechanisms (the BSS and the CES) obviously capable of producing runaways. The spread in abundances over a range of about 1 dex surely reflects the range in the Galactocentric distance of the birthplaces of the stars before they are ejected into the halo and the presence of an abundance gradient in the Galaxy. Consideration of either the

projected rotational velocities or the radial velocities cannot provide a determination of the relative probabilities of the BSS and the CES in providing the runaway B stars. But an intensive search for binaries among the B runaway population may yet shed light on the relative contributions of the BSS and the CES. The ability to identify runaway stars formed by the BSS will be enhanced by extending the non-LTE analysis to other elements, notably O and S, which appear to have large excesses in [X/Fe] in the (few) LMXB secondaries analyzed for this pair of elements.

References

Abt, H. A., Levato, H., & Grosso, M. 2002, ApJ, 573, 359
Abt, H. A., & Levy, S. G. 1978, ApJS, 36, 241
Aerts, C., De Cat, P., De Ridder, J., et al. 2006, A&A, 449, 305
Ballester, P., Modigliani, A., Boitquin, O., et al. 2000, Msngr, 101, 31
Barbier-Brossat, M., & Figon, P. 2000, A&AS, 142, 217
Behr, B. B. 2003, ApJS, 149, 101
Blaauw, A. 1961, BAN, 15, 265
Blaauw, A. 1993, in ASP Conf. Ser. 35, Massive Stars: Their Lives in the Interstellar Medium, ed. J. P. Cassinelli & E. B. Churchwell (San Francisco, CA: ASP), 207
Blaauw, A., & Morgan, W. W. 1954, ApJ, 119, 625
Brott, I., de Mink, S. E., Cantiello, M., et al. 2011, A&A, 530, A115
Brown, W. R. 2015, ARA&A, 53, 15
Daflon, S., & Cunha, K. 2004, ApJ, 617, 1115
Daflon, S., Cunha, K., de la Reza, R., Holtzman, J., & Chiappini, C. 2009, AJ, 138, 1577
de Bruijne, J. H. J., & Eilers, A.-C. 2012, A&A, 546, A61
de Zeeuw, T., Hoogerwerf, R., & de Bruijne, J. 2001, in ASP Conf. Ser. 228, Dynamics of Star Clusters and the Milky Way, ed. S. Deiters et al. (San Francisco, CA: ASP), 201
Dekker, H., D'Odorico, S., Kaufer, A., Delabre, B., & Kotzlowski, H. 2000, Proc. SPIE, 4008, 534
Duflot, M., Figon, P., & Meyssonnier, N. 1998, yCat, 3190
Dufton, P. L., Ryans, R. S. I., Trundle, C., et al. 2005, A&A, 434, 1125
Dunstall, P. R., Dufton, P. L., Sana, H., et al. 2015, A&A, 580, A93
Dyson, J. E., & Hartquist, T. W. 1983, MNRAS, 203, 1233
Fraser, M., Dufton, P. L., Hunter, I., & Ryans, R. S. I. 2010, MNRAS, 404, 1306
Garmany, C. D., Conti, P. S., & Massey, P. 1980, ApJ, 242, 1063
Gies, D. R., & Bolton, C. T. 1986, ApJS, 61, 419
Gontcharov, G. A. 2006, AstL, 32, 759
González Hernández, J. I., Rebolo, R., & Israelian, G. 2008, A&A, 478, 203
Greenstein, J. L., & Sargent, A. I. 1974, ApJS, 28, 157
Guthrie, B. N. G. 1984, MNRAS, 210, 159
Gvaramadze, V. V., Gualandris, A., & Portegies Zwart, S. 2009, MNRAS, 396, 570
Heber, U., Edelmann, H., Napiwotzki, R., Altmann, M., & Scholz, R.-D. 2008, A&A, 483, L21

Hoffer, J. B. 1983, AJ, 88, 1420
Hoogerwerf, R., de Bruijne, J. H. J., & de Zeeuw, P. T. 2001, A&A, 365, 49
Huang, Y., Liu, X.-W., Zhang, H.-W., et al. 2015, RAA, 15, 1240
Hubeny, I. 1988, CoPhC, 52, 103
Hubeny, I., Heap, S. R., & Lanz, T. 1998, in ASP Conf. Ser. 131, Properties of Hot Luminous Stars, ed. I. Howarth (San Francisco, CA: ASP), 108
Hubeny, I., & Lanz, T. 1995, ApJ, 439, 875
Hunter, I., Brott, I., Langer, N., et al. 2009, A&A, 496, 841
Hunter, I., Brott, I., Lennon, D. J., et al. 2008, ApJL, 676, L29
Hunter, I., Dufton, P. L., Smartt, S. J., et al. 2007, A&A, 466, 277
Irrgang, A., Przybilla, N., Heber, U., Nieva, M. F., & Schuh, S. 2010, ApJ, 711, 138
Kaufer, A., Stahl, O., Tubbesing, S., et al. 1999, Msngr, 95, 8
Keenan, F. P., Dufton, P. L., & McKeith, C. D. 1982, MNRAS, 200, 673
Kharchenko, N. V., Piskunov, A. E., & Scholz, R.-D. 2004, AN, 325, 439
Kharchenko, N. V., Scholz, R.-D., Piskunov, A. E., Röser, S., & Schilbach, E. 2007, AN, 328, 889
Kilkenny, D., & Hill, P. W. 1975, MNRAS, 172, 649
Kordopatis, G., Gilmore, G., Steinmetz, M., et al. 2013, AJ, 146, 134
Lanz, T., & Hubeny, I. 2007, ApJS, 169, 83
Leonard, P. J. T. 1989, AJ, 98, 217
Leonard, P. J. T. 1993, in ASP Conf. Ser. 45, Luminous High-Latitude Stars, ed. D. D. Sasselov (San Francisco, CA: ASP), 360
Leonard, P. J. T., & Duncan, M. J. 1990, AJ, 99, 608
Leonard, P. J. T., & Fahlman, G. G. 1991, AJ, 102, 994
Luck, R. E., & Lambert, D. L. 2011, AJ, 142, 136
Lyubimkov, L. S., Lambert, D. L., Poklad, D. B., Rachkovskaya, T. M., & Rostopchin, S. I. 2013, MNRAS, 428, 3497
Lyubimkov, L. S., Rostopchin, S. I., Rachkovskaya, T. M., Poklad, D. B., & Lambert, D. L. 2005, MNRAS, 358, 193
Magee, H. R. M., Dufton, P. L., Keenan, F. P., et al. 1998, A&A, 338, 85
Martin, J. C. 2003, PASP, 115, 49
Martin, J. C. 2004, AJ, 128, 2474
Martin, J. C. 2006, AJ, 131, 3047
McDonald, I., Zijlstra, A. A., & Boyer, M. L. 2012, MNRAS, 427, 343
McEvoy, C. M., Dufton, P. L., Evans, C. J., et al. 2015, A&A, 575, A70
Mdzinarishvili, T. G., & Chargeishvili, K. B. 2005, A&A, 431, L1
Nieva, M. F., & Przybilla, N. 2006, ApJL, 639, L39
Nieva, M. F., & Przybilla, N. 2008, A&A, 481, 199
Nieva, M.-F., & Simón-Díaz, S. 2011, A&A, 532, A2
Philp, C. J., Evans, C. R., Leonard, P. J. T., & Frail, D. A. 1996, AJ, 111, 1220
Portegies Zwart, S. F. 2000, ApJ, 544, 437
Poveda, A., Ruiz, J., & Allen, C. 1967, BOTT, 4, 86
Przybilla, N., Fernanda Nieva, M., Heber, U., & Butler, K. 2008, ApJL, 684, L103
Puls, J., Urbaneja, M. A., Venero, R., et al. 2005, A&A, 435, 669
Rolleston, W. R. J., Hambly, N. C., Dufton, P. L., et al. 1997, MNRAS, 290, 422
Rolleston, W. R. J., Smartt, S. J., Dufton, P. L., & Ryans, R. S. I. 2000, A&A, 363, 537
Ryans, R. S. I., Dufton, P. L., Mooney, C. J., et al. 2003, A&A, 401, 1119
Sadakane, K., Arai, A., Aoki, W., et al. 2006, PASJ, 58, 595
Sana, H., de Koter, A., de Mink, S. E., et al. 2013, A&A, 550, A107
Santolaya-Rey, A. E., Puls, J., & Herrero, A. 1997, A&A, 323, 488
Sayer, R. W., Nice, D. J., & Kaspi, V. M. 1996, ApJ, 461, 357
Shaver, P. A., McGee, R. X., Newton, L. M., Danks, A. C., & Pottasch, S. R. 1983, MNRAS, 204, 53
Silva, M. D. V., & Napiwotzki, R. 2011, MNRAS, 411, 2596
Simón-Díaz, S., Herrero, A., Uytterhoeven, K., et al. 2010, ApJL, 720, L174
Smartt, S. J., Dufton, P. L., & Lennon, D. J. 1997, A&A, 326, 763
Tetzlaff, N., Neuhäuser, R., & Hohle, M. M. 2011, MNRAS, 410, 190
Tobin, W. 1987, in IAU Coll. 95: Second Conf. on Faint Blue Stars, ed. A. G. D. Philip, D. S. Hayes, & J. W. Liebert (Schenectady, NY: L. Davis Press), 149
Trundle, C., Dufton, P. L., Hunter, I., et al. 2007, A&A, 471, 625
Tull, R. G., MacQueen, P. J., Sneden, C., & Lambert, D. L. 1995, PASP, 107, 251
Wolff, S. C., Edwards, S., & Preston, G. W. 1982, ApJ, 252, 322
Zwicky, F. 1957, Morphological Astronomy (Berlin: Springer)